

Article

# Biogas Upgrading Via Dry Reforming Over a Ni-Sn/CeO<sub>2</sub>-Al<sub>2</sub>O<sub>3</sub> Catalyst: Influence of the Biogas Source

Estelle le Saché , Sarah Johnson, Laura Pastor-Pérez , Bahman Amini Horri and Tomas R. Reina \* 

Chemical & Process Engineering Department, University of Surrey, Guildford GU2 7XH, UK; e.lesache@surrey.ac.uk (E.I.S.); sj00174@surrey.ac.uk (S.J.); l.pastorperez@surrey.ac.uk (L.P.-P.); b.aminihorri@surrey.ac.uk (B.A.H.)

\* Correspondence: t.ramirezreina@surrey.ac.uk; Tel.: +44-148-368-6597

Received: 15 February 2019; Accepted: 13 March 2019; Published: 15 March 2019



**Abstract:** Biogas is a renewable, as well as abundant, fuel source which can be utilised in the production of heat and electricity as an alternative to fossil fuels. Biogas can additionally be upgraded via the dry reforming reactions into high value syngas. Nickel-based catalysts are well studied for this purpose but have shown little resilience to deactivation caused by carbon deposition. The use of bi-metallic formulations, as well as the introduction of promoters, are hence required to improve catalytic performance. In this study, the effect of varying compositions of model biogas (CH<sub>4</sub>/CO<sub>2</sub> mixtures) on a promising multicomponent Ni-Sn/CeO<sub>2</sub>-Al<sub>2</sub>O<sub>3</sub> catalyst was investigated. For intermediate temperatures (650 °C), the catalyst displayed good levels of conversions in a surrogate sewage biogas (CH<sub>4</sub>/CO<sub>2</sub> molar ratio of 1.5). Little deactivation was observed over a 20 h stability run, and greater coke resistance was achieved, related to a reference catalyst. Hence, this research confirms that biogas can suitably be used to generate H<sub>2</sub>-rich syngas at intermediate temperatures provided a suitable catalyst is employed in the reaction.

**Keywords:** biogas; syngas production; DRM; Ni catalyst; bi-metallic catalyst; ceria-alumina

## 1. Introduction

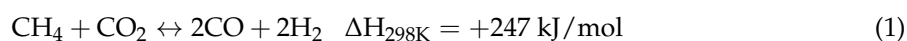
Rising greenhouse gas (GHG) emissions and the associated global warming threat are some of the largest challenges facing the world today. The energy sector alone accounts for two-thirds of total greenhouse gas emissions, and around 80% of carbon dioxide emissions [1]. The majority of CO<sub>2</sub> emissions are produced from the combustion of fossil fuels for the generation of energy, and from other industrial processes. With global energy demand growing rapidly, the need for the decarbonisation of the energy industry has never been greater. Although CO<sub>2</sub> is the primary greenhouse gas emitted, the detrimental impact of releasing methane, with a global warming potential (GWP) of 25 [2], into the atmosphere should not be underestimated.

In recent years, more efforts have been made by national governments to implement GHG mitigating processes and technologies, such as carbon capture and storage. However, there is still much to be done to meet the target agreed on by ‘The Paris Agreement’ of limiting the global average temperature to below 2 °C above pre-industrial levels. Therefore, it is crucial to redirect the global focus from fossil fuels to renewable energy sources in order to minimise the destructive effects of climate change.

Biogas is one possible source of renewable energy and is commonly referred to as a gaseous mixture of methane and carbon dioxide produced by the anaerobic digestion of biodegradable matter.

Typical feedstocks for biogas are waste materials, such as municipal waste, sewage sludge and agricultural waste. Other components present in biogas include water vapour, nitrogen and hydrogen sulphide. However, the actual composition, as well as the  $\text{CH}_4/\text{CO}_2$  ratio, differs depending on the type of feedstock and the digestion process used [3]. Although biogas is the main renewable energy source contributing to the global energy supply [4], technical challenges still prevent it from being fully utilised for the generation of electricity.

Alternatively, biogas can be converted into high value syngas, a gaseous mixture of carbon monoxide and hydrogen, via the dry reforming of methane (DRM), as shown in Equation (1).



Syngas is an extremely useful intermediate as it is used as a precursor to synthesise valuable fuels and chemicals such as methanol, as well as long chained hydrocarbons via the Fischer–Tropsch process [5,6]. Furthermore, syngas has been suggested as a feed gas to high temperature solid oxide fuel cells (SOFCs) with either internal or external reforming to generate electricity [7–9]. Figure 1 illustrates the opportunity to generate renewable energy from organic waste by combining anaerobic digestion with DRM and SOFCs. The high operating temperatures of SOFCs makes direct internal reforming feasible. However, the direct use of biogas in SOFCs is still associated with carbon deposition and sulphur poisoning in the fuel cell anode, which weakens cell durability and causes loss of cell performance [10].

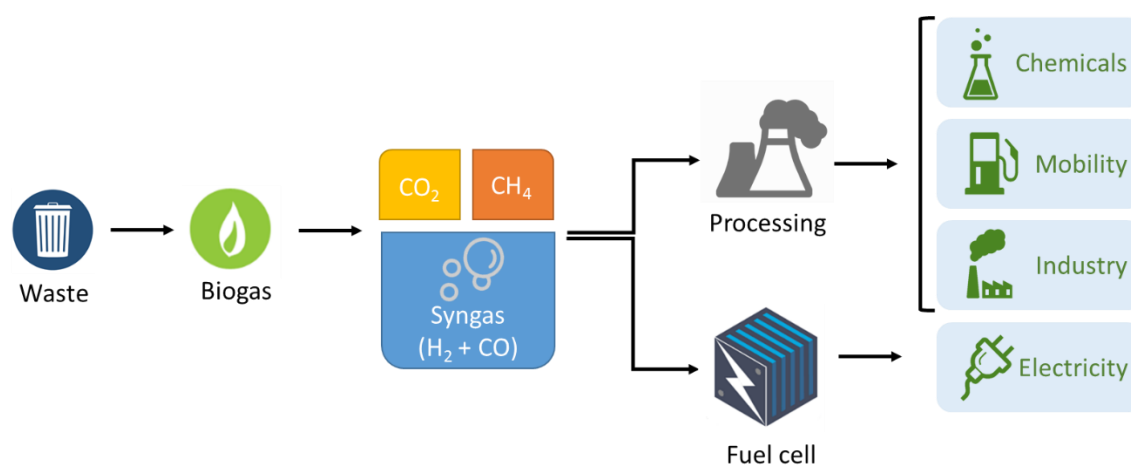
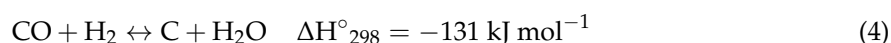
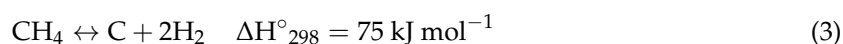
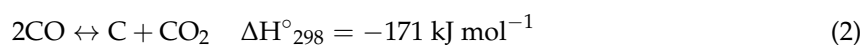


**Figure 1.** Block flow diagram illustrating the potential of utilising organic waste to generate 'green energy'.

Due to the endothermic nature of the dry reforming reaction and the high stability of the reactants, high reaction temperatures and a stable catalyst are required to achieve high syngas yields [11]. However, high reaction temperatures often lead to the deactivation of the catalyst. Deactivation is caused by either solid carbon deposition forming on the catalyst, which physically blocks the active metal phase and is known as coking, or through sintering of the catalyst active phase at high temperatures. There are a number of side reactions which are responsible for the formation of carbon, and hence negatively affect the performance of the catalyst. In dry reforming, carbon is most commonly produced by the Boudouard reaction, as shown in Equation (2), methane decomposition, as shown in Equation (3) as well as carbon monoxide reduction, as shown in Equation (4).



Therefore, an effective dry reforming catalyst needs to be thermally stable in order to be resistant to coking and sintering, whilst yielding optimal conversions. Additionally, it must be economically viable so that it can be cost effectively scaled-up for industrial applications. All these factors are heavily dependent on the selected active metal, as well as the properties of the support and/or promoter [5].

Nickel-based materials are widely regarded as effective catalysts for the dry reforming of methane as they display good activity and respectable conversions [12]. However, the main drawback of Ni-based catalysts is that they suffer from quick deactivation as a result of carbon deposition and an inclination to sintering. Noble metal-based catalysts are frequently cited as a superior alternative due to greater stability and higher resilience to coking. Catalysts based on Ru and Rh in particular show higher activity compared to nickel [13]. Despite this, noble metal catalysts are far more expensive and have limited availability in comparison to Ni-based ones and are therefore unfeasible for use in industrial applications.

In order to develop a stable, high performing nickel-based catalyst, the material is often upgraded using an appropriate support or adding a promoter. Alumina ( $\text{Al}_2\text{O}_3$ )-based supports have been thoroughly investigated due to their high specific area which improves metal dispersion [14]. Yet implementing alumina as a support is still associated with catalyst deactivation, caused mainly by coke formation on the acid sites [14]. To combat this problem, basic promoters such as ceria ( $\text{CeO}_2$ ) can be used to stabilise the support. It has been shown that Ni catalysts supported on  $\text{CeO}_2$ - $\text{Al}_2\text{O}_3$  systems showed far better performance than either  $\text{CeO}_2$  or  $\text{Al}_2\text{O}_3$  supported nickel catalysts [15]. Indeed, ceria not only tunes the acid/base properties of the support but also provides excellent oxygen mobility (due to its high oxygen storage capacity), thus helping to prevent coking via oxidation of the coke precursors [16].

Moreover, bi-metallic systems can further enhance catalytic performance; the addition of a second metal has shown to improve the activity, as well as the stability of the catalyst [17–19]. It is believed that this is related to the metal–metal interactions which reduce the electron donor capacity of the active metal, limiting its tendency to form strong bonds with carbon precursors [20,21]. As recently demonstrated by Stroud et al., bi-metallic Ni-Sn supported  $\text{Al}_2\text{O}_3$  and  $\text{CeO}_2$ - $\text{Al}_2\text{O}_3$  catalysts can effectively generate good conversions for DRM whilst exhibiting high stability [16]. The positive effect of Sn as an added metal to Ni was further investigated by Guharoy et al. in a DFT study concluding that the beneficial effect of tin is credited to Sn atoms occupying C nucleation sites in the vicinity on Ni atoms, slowing coke formation (i.e., increasing the energy barrier for coke nucleation) [22].

Under these premises, the aim of this work is to investigate the performance of an optimised multicomponent Ni-Sn/ $\text{CeO}_2$ - $\text{Al}_2\text{O}_3$  catalyst for the production of syngas from a biogas feed via the dry reforming of methane. The impact of the type of biogas and more precisely its origin (i.e., sewage, municipal waste, landfill and organic waste) is also a subject of this study which aims to showcase a suitable upgrading route for different types of biogases via reforming reactions.

## 2. Materials and Methods

### 2.1. Catalyst Preparation

The Ni-Sn/ $\text{CeO}_2$ - $\text{Al}_2\text{O}_3$  catalyst was synthesised by sequential impregnation. First, the ceria promoted support was prepared by impregnation of the correct amount of  $\text{Ce}(\text{NO}_3)_2 \cdot 6\text{H}_2\text{O}$  (Sigma-Aldrich) on  $\gamma$ - $\text{Al}_2\text{O}_3$  powder (Sasol) in order to obtain a 20 wt % loading of  $\text{CeO}_2$ . After 1 h of stirring, the solvent, acetone, was evaporated at reduced pressure in a rotary evaporator. The resulting powder was dried overnight at 80 °C and calcined at 800 °C for 4 h. The support was then impregnated in the same way with the necessary amount of  $\text{Ni}(\text{NO}_3)_2 \cdot 6\text{H}_2\text{O}$  (Sigma-Aldrich) dissolved in acetone, to achieve a 10 wt % metal loading. Lastly, the obtained solid was impregnated with  $\text{SnCl}_2$  (Sigma-Aldrich) following the same procedure to achieve a Sn/Ni molar ratio of 0.02. This ratio was chosen based on previous work [16]. For simplicity the catalyst will be referred to as Ni-Sn/CeAl from here on.

## 2.2. Catalyst Characterisation

N<sub>2</sub>-adsorption-desorption analysis was performed in a QuadraSorb Station 4 at liquid nitrogen temperature. Prior to the analysis, the catalyst was degassed at 250 °C for 4 h in vacuum. The surface area was calculated from the Brunauer–Emmett–Teller (BET) equation.

X-ray fluorescence (XRF) analysis of the catalyst was carried out on an EDAX Eagle III spectrophotometer using rhodium as the radiation source.

X-ray diffraction (XRD) analysis was conducted on fresh and spent samples using an X'Pert Powder instrument from PANalytical. The diffraction patterns were recorded over a 2θ range of 10 to 90°. A step size of 0.05° was used with a time step of 450 s. Diffraction patterns were recorded at 30 mA and 40 kV, using Cu Kα radiation (λ = 0.154 nm).

Temperature-programmed reduction (TPR) in hydrogen was carried out on the calcined sample in a U-shaped quartz cell using a 5% H<sub>2</sub>/He gas flow of 50 mL·min<sup>-1</sup>, with a heating rate of 10 °C min<sup>-1</sup>. Prior to analysis the catalyst was treated with He at 150 °C for 1 h. Hydrogen consumption was measured by on-line mass spectrometry (Pfeiffer, OmniStar GSD 301).

Thermogravimetric analysis (DSC-TGA) was carried out on the samples post stability test in an SDT Q600 V8 from TA Instruments. The samples were ramped from room temperature to 900 °C at 10 °C min<sup>-1</sup> in air.

## 2.3. Catalytic Activity

The catalytic performance for the dry reforming of methane at varying compositions of model biogas (CH<sub>4</sub> and CO<sub>2</sub>) was carried out in a continuous flow quartz tube reactor (10 mm ID) equipped with a thermocouple, at atmospheric pressure. Reactants and products were followed by an on-line gas analyser (ABB AO2020). In order to achieve a weight hourly space velocity (WHSVs) of 30 L g<sup>-1</sup> h<sup>-1</sup>, a mass of 0.2 g of catalyst was used for each screening. All samples were pre-reduced in situ using 100 mL·min<sup>-1</sup> of 10% H<sub>2</sub> in N<sub>2</sub> at 850 °C for 1 h.

Reactions were conducted using a total flow of 100 mL·min<sup>-1</sup> of varying biogas compositions for temperatures ranging from 550 to 850 °C in 50 °C increments. The catalytic performance was measured for CH<sub>4</sub>/CO<sub>2</sub> molar ratios of 1, 1.25, 1.5 and 1.85 balanced in N<sub>2</sub>. These ratios were carefully chosen in order to model DRM of biogas produced from a range of residues [23]. Table 1 lists the types of biogas source, as well as the corresponding CH<sub>4</sub> and CO<sub>2</sub> content, being modelled by the specific CH<sub>4</sub>/CO<sub>2</sub> molar ratio selected for each reaction.

**Table 1.** List of biogas sources and the corresponding methane and carbon dioxide content, and the resulting CH<sub>4</sub>/CO<sub>2</sub> molar ratio. Adapted from Lau et al. [23].

Biogas Source	CH <sub>4</sub> Content (%)	CO <sub>2</sub> Content (%)	CH <sub>4</sub> /CO <sub>2</sub> Molar Ratio
Model Composition	50	50	1:1
Landfill Waste	55	45	1.25
Sewage Waste	60	40	1.5
Organic Waste	65	35	1.85

Lastly, stability tests were carried out on Ni-Sn/CeAl and a reference nickel on alumina with the same Ni loading (Ni/Al) catalyst using CH<sub>4</sub>/CO<sub>2</sub> molar ratio of 1 and 1.5 and a temperature of 650 °C for 20 h. The low temperature was chosen in order to simulate a syngas suitable for direct use in intermediate temperature SOFCs aiming for the hypothetical utilisation of biogas in an internal reforming SOFC.

Conversions of the reactants, as well as the H<sub>2</sub>/CO ratio and H<sub>2</sub> yields, were calculated for each run to determine the effect of varying the biogas composition on the performance of the catalyst as follows:

$$X_{\text{CH}_4}(\%) = 100 * \frac{[\text{CH}_4]_{\text{In}} - [\text{CH}_4]_{\text{Out}}}{[\text{CH}_4]_{\text{In}}} \quad (5)$$

$$X_{\text{CO}_2}(\%) = 100 * \frac{[\text{CO}_2]_{\text{In}} - [\text{CO}_2]_{\text{Out}}}{[\text{CO}_2]_{\text{Out}}} \quad (6)$$

$$\text{H}_2/\text{CO ratio} = \frac{[\text{H}_2]_{\text{Out}}}{[\text{CO}]_{\text{Out}}} \quad (7)$$

$$Y_{\text{H}_2}(\%) = 100 * \frac{[\text{H}_2]_{\text{Out}}}{2[\text{CH}_4]_{\text{In}}} \quad (8)$$

### 3. Results and Discussion

#### 3.1. Physicochemical Properties

The N<sub>2</sub> adsorption-desorption isotherm of the calcined catalyst is shown in Figure 2. The analysis generated a type IV isotherm with a characteristic hysteresis loop, which is associated with the presence of well-developed cylindrical mesopores. The steepness of the loop suggests that the mesopores were homogeneously distributed throughout the structure of the sample [24].

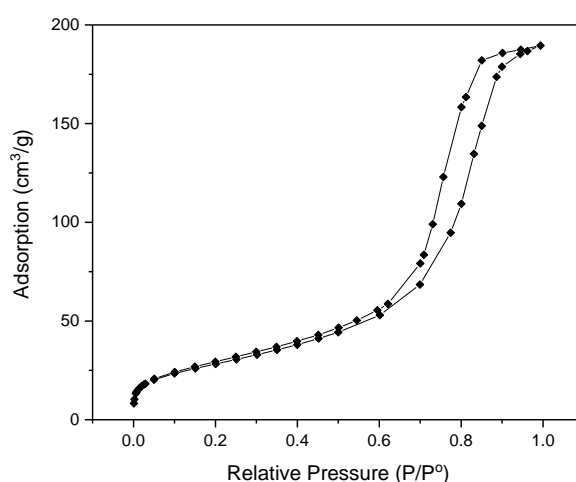


**Figure 2.** Nitrogen adsorption-desorption isotherm of Ni-Sn/CeAl sample.

The surface area, calculated using the BET method, the total pore volume and the average pore diameter of the calcined catalyst are listed in Table 2 along with its elemental composition determined by XRF. Although the textural properties were primarily governed by the  $\gamma$ -Al<sub>2</sub>O<sub>3</sub> support, the surface area and pore volume measured were smaller than that of the support itself due to CeO<sub>2</sub> and Ni particles present on the surface and covering the pores [25]. The metal content of the obtained catalyst was very close to the intended value.

**Table 2.** Textural properties of Ni-Sn/CeAl post calcination as determined by the Brunauer–Emmett–Teller (BET) equation and X-ray fluorescence (XRF) analysis.

	NiO wt %	Sn wt %	S <sub>BET</sub> (m <sup>2</sup> ·g <sup>-1</sup> )	V <sub>Pore</sub> (cm <sup>3</sup> ·g <sup>-1</sup> )	D <sub>Pore</sub> (nm)
Ni-Sn/CeAl	10.3	1.3	103	0.31	8.3
CeAl	-	-	130	0.34	9.6

#### 3.2. Reducibility: H<sub>2</sub>-TPR

The temperature programmed reduction was conducted in order investigate the interactions between the support and metallic species, as well as the redox properties of the catalyst which are essential for DRM [5]. Figure 3 shows the H<sub>2</sub>-TPR profile of the calcined catalyst. The Ni-Sn/CeAl sample presents a main reduction peak at around 820 °C. This high reduction temperature is attributed

to the reduction of  $\text{Ni}^{2+}$  to Ni, strongly interacting with the alumina support. The high reduction temperature may indicate the presence of  $\text{NiAl}_2\text{O}_4$  spinel, which is difficult to reduce and is associated with high reduction temperatures of 600–870 °C [16,26]. It appears that a second reduction process occurs at 900 °C, possibly due to the reduction of  $\text{CeO}_2$  and  $\text{Al}_2\text{O}_3$  to  $\text{CeAlO}_3$ , in good agreement with the XRD results that will be discussed later in the paper [27,28].

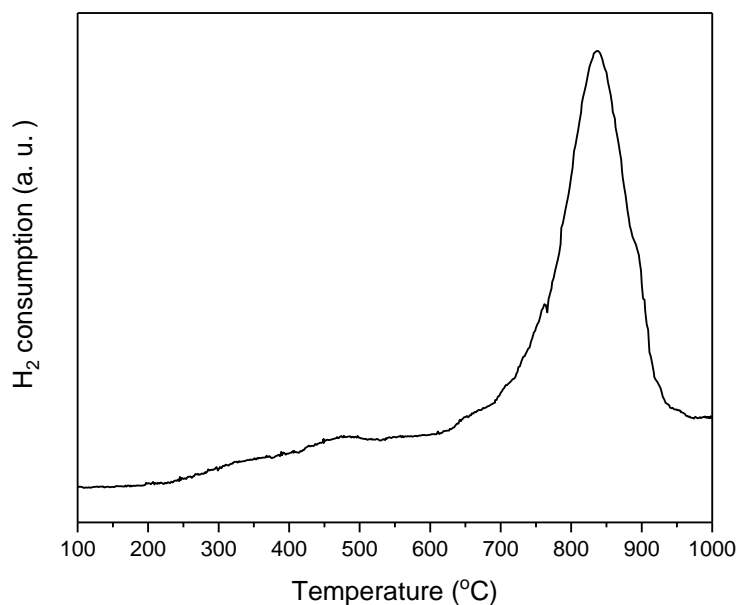
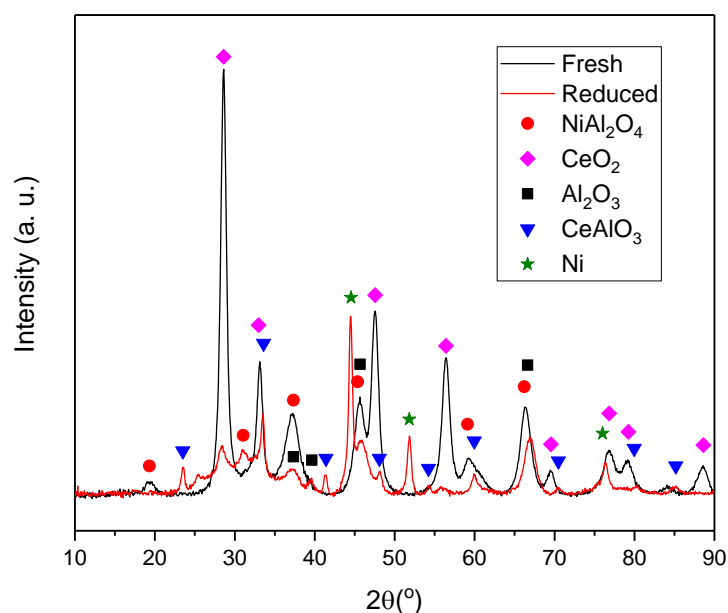


Figure 3.  $\text{H}_2$ -TPR profile of Ni-Sn/CeAl.

### 3.3. XRD

The structural properties of the Ni-Sn/CeAl catalyst after calcination (fresh) and after reduction under  $\text{H}_2$  at 850 °C for 1 hour were determined and the XRD profiles are shown in Figure 4. The fresh catalyst profile shows no presence of characteristic crystalline peaks associated to Sn or  $\text{SnO}_x$  due to the low amount used, metallic nickel ( $\text{Ni}^0$ ) or oxidised nickel (NiO) species. The profile presents, however, peaks related to  $\gamma\text{-Al}_2\text{O}_3$  (JCPDS# 00-048-0367) and  $\text{NiAl}_2\text{O}_4$  (JCPDS# 00-010-0339). Although  $\gamma\text{-Al}_2\text{O}_3$  and  $\text{NiAl}_2\text{O}_4$  phases are hardly distinguishable due to their broad and overlapping diffraction peaks, the formation of nickel aluminate spinel ( $\text{NiAl}_2\text{O}_4$ ) can be identified due to the slight shifts towards smaller angles of three strong diffraction peaks associated with  $\gamma\text{-Al}_2\text{O}_3$ : at  $2\theta$  37.0°, 45.5° and 66.3° [27]. Indeed, the nickel aluminate spinel can be formed at high calcination temperature (800 °C) via the reaction between NiO and  $\text{Al}_2\text{O}_3$ . Additionally, for the full formation of aluminate spinel, a Ni loading of around 33 wt % is necessary [29], therefore, since the Ni loading in this sample was much lower it is most likely that  $\text{NiAl}_2\text{O}_4$  spinel co-exists with Ni nanoparticles supported on the  $\gamma\text{-Al}_2\text{O}_3$  support.



**Figure 4.** XRD profiles of the fresh and reduced Ni-Sn/CeAl catalyst.

The fresh sample presents, as well, the typical diffraction peaks of  $\text{CeO}_2$  fluorite cubic cells (JCPDS# 01-075-0390) at  $28.5^\circ$ ,  $33.1^\circ$ ,  $47.8^\circ$  and  $56.3^\circ$ . However, once the sample was reduced, an additional  $\text{CeAlO}_3$  tetragonal phase (JCPDS# 01-081-1185) was detected. When reduced at temperatures above  $600^\circ\text{C}$ ,  $\text{Ce}_2\text{O}_3$  and  $\gamma\text{-Al}_2\text{O}_3$  reacted to produce  $\text{CeAlO}_3$  in good agreement with the results discussed in the TPR section [28]. However not all  $\text{CeO}_x$  species were reacted to  $\text{CeAlO}_3$  since traces of  $\text{CeO}_2$  cubic phase can still be detected at  $28.5^\circ$ . Finally, the XRD pattern of the sample reduced in hydrogen shows the presence of metallic Ni particles (JCPDS# 87-0712), which indicates that  $\text{Ni}^0$  will be the predominant active phase for the dry reforming reaction. The shift towards the higher angles of the  $37.0^\circ$ ,  $45.5^\circ$  and  $66.3^\circ$  peaks confirms that  $\text{NiAl}_2\text{O}_4$  has been reduced to Ni metallic and  $\gamma\text{-Al}_2\text{O}_3$  upon reduction at  $850^\circ\text{C}$ , confirming the TPR results.

### 3.4. Catalyst Performance

The catalytic performance for DRM was studied over a range of temperatures ( $550\text{--}850^\circ\text{C}$ ) at  $\text{CH}_4/\text{CO}_2$  molar ratios of 1, 1.25, 1.5 and 1.85. The effect of varying the biogas feed concentration, in terms of  $\text{CH}_4$  conversion as a function of temperature, is reported in Figure 5a. It was shown that with increasing methane concentration, the overall  $\text{CH}_4$  conversion decreases. Indeed, methane was introduced in excess for DRM. Additionally,  $\text{CH}_4$  conversion increased with temperature; this aligns with expectations, as the endothermic nature of the reaction requires higher temperatures to reach equilibrium conversion. Hence, superior activity of the catalyst was observed during the temperature screening at a 1:1 molar ratio of  $\text{CH}_4/\text{CO}_2$ , which reached a methane conversion of 93% at  $850^\circ\text{C}$ .

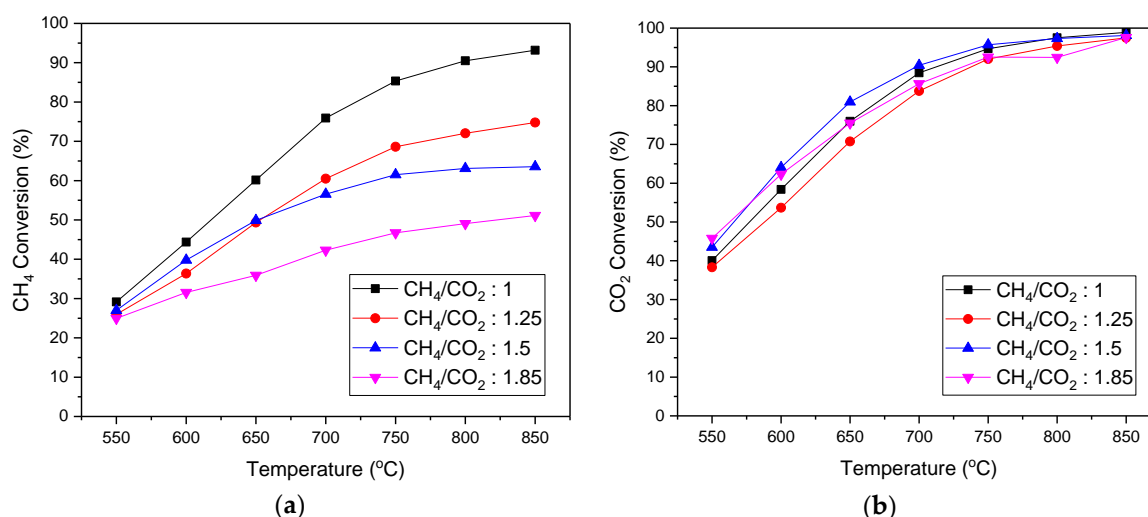


**Figure 5.** Catalytic performance of Ni-Sn/CeAl at CH<sub>4</sub>/CO<sub>2</sub> molar ratios of 1, 1.25, 1.5 and 1.85 as a function of temperature: (a) methane conversion; (b) carbon dioxide conversion.

Figure 5b shows the conversion of CO<sub>2</sub> as a function of temperature for various biogas compositions. The temperature screening carried out at CH<sub>4</sub>/CO<sub>2</sub> molar ratio of 1.5 displayed the highest conversion for most temperatures. For all ratios, the highest CO<sub>2</sub> conversion was achieved at 850 °C, reaching around 98%. Overall, the conversion witnessed for CO<sub>2</sub> was much higher than that of CH<sub>4</sub>; CO<sub>2</sub> being the limiting reactant for ratios greater than 1. For the model biogas mixture (CH<sub>4</sub>/CO<sub>2</sub> = 1) however, CH<sub>4</sub> and CO<sub>2</sub> conversions should be similar. The fact that CO<sub>2</sub> conversion was slightly higher than CH<sub>4</sub> conversion for temperatures lower than 850 °C was due to the occurrence of the reverse water gas shift (RWGS) reaction, consuming CO<sub>2</sub> and H<sub>2</sub> to form CO as previously reported elsewhere [5]. This can also be attributed to the high activation energy of methane [11,22].

The effect of varying the biogas feed concentration on the H<sub>2</sub>/CO ratio is illustrated in Figure 6a. As a general rule, the H<sub>2</sub>/CO ratio increased with higher temperatures, with the exception of the temperature screening carried out at a CH<sub>4</sub>/CO<sub>2</sub> molar ratio of 1.85, where the H<sub>2</sub>/CO ratio initially decreased with the increment of the temperature and only increased once a temperature of 650 °C was reached. The high concentration of hydrogen in the products stream may be explained by the excess of methane in the feed gas. It is likely that this excess created favourable conditions for the methane decomposition reaction to take place, which contributed to a higher concentration (partial pressure) of H<sub>2</sub> at lower temperatures. Furthermore, it was observed that at lower temperatures (550–600 °C), a larger CH<sub>4</sub>/CO<sub>2</sub> ratio yielded a higher H<sub>2</sub>/CO ratio. Whereas, at higher temperatures (700–850 °C), the H<sub>2</sub>/CO ratio exhibited the largest value for a model biogas feed of 1:1 molar ratio of CH<sub>4</sub>/CO<sub>2</sub>.

The H<sub>2</sub> yield obtained for each biogas composition as a function of temperature is shown in Figure 6b. As expected, yields increased along with temperature and CH<sub>4</sub> conversion. As the CH<sub>4</sub>/CO<sub>2</sub> molar ratio increased, H<sub>2</sub> yields decreased due to excess CH<sub>4</sub> in the feed and reduced CH<sub>4</sub> conversion.

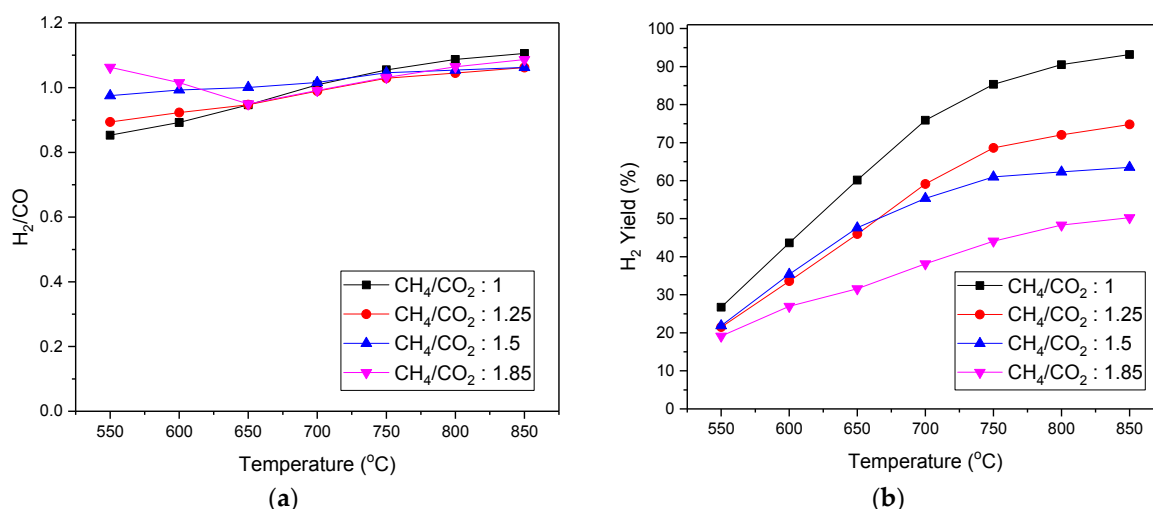


**Figure 6.** (a)  $H_2/CO$  ratio and (b)  $H_2$  yield for Ni-Sn/CeAl at  $CH_4/CO_2$  molar ratios of 1, 1.25, 1.5 and 1.85 as a function of temperature.

In order to establish a more general comparison with previously reported Ni-based catalysts for biogas reforming reactions, different reported catalysts and the conditions used in the biogas dry reforming are presented in Table 3. As shown in the table, our Ni-Sn/CeAl catalyst can be deemed to perform with superior behaviour in the compared conditions, especially in terms of hydrogen yields. Furthermore, our catalyst continues showing a good performance tested at lower temperatures and long-term tests, which reinforces the exceptional behaviour of the developed system.

**Table 3.** Catalysts employed, and conditions used in catalytic biogas dry reforming, using  $CH_4/CO_2$  ratio: 1.5. WHSV: weight hourly space velocity.

	Temperature (°C)	WHSV ( $L \cdot g^{-1} \cdot h^{-1}$ )	$CH_4$ Conversion (%)	$CO_2$ Conversion (%)	$H_2$ Yield (%)	Reference
Ni/MgO	800	60	62.2	92.3	52.6	[30]
Ni/Ce- $Al_2O_3$	800	60	59.3	77.8	57.1	[30]
Ni/Zr- $Al_2O_3$	800	60	58.4	73.5	51.9	[30]
Ni/Ce-Zr- $Al_2O_3$	800	60	64.5	85.6	57.5	[30]
Rh-Ni/Ce- $Al_2O_3$	800	60	60.1	94.4	63.3	[30]
Ni/ $Al_2O_3$	800	120	60.0	83.0	48.0	[14]
Ni/Ce- $Al_2O_3$	800	120	63.0	89.0	50.0	[14]
Ni/La- $Al_2O_3$	800	120	69.0	94.0	57.0	[14]
Ni/Ce-La- $Al_2O_3$	800	120	69.0	94.5	58.0	[14]
Ni/CaO- $Al_2O_3$	800	120	57.9	75.2	30.5	[6]
Ni/MgO- $Al_2O_3$	800	120	57.7	75.2	32.4	[6]
Reformax <sup>®</sup> 250	750	18	64.0	86.0	28.8	[31]
Ni-Sn/Ce- $Al_2O_3$	800	30	63.1	97.5	62.3	This work
Equilibrium	800	-	65.5	99.1	65.2	

### 3.5. Stability Test

Long-term stability tests were carried out at a temperature of 650 °C. The temperature was selected in order to simulate a syngas suitable for direct use in intermediate temperature SOFCs.

The results of the stability tests are displayed in Figure 7, which shows both  $CH_4$  and  $CO_2$  conversion as a function of time. Figure 7a compares the stability of Ni-Sn/CeAl under two biogas mixtures: 1 and 1.5  $CH_4/CO_2$  molar ratios. When tested with the model biogas mixture, the catalyst showed good performance with 79%  $CO_2$  conversion and 60%  $CH_4$  conversion. The performance was stable with a slight deactivation equivalent to 5% conversion loss. On the other hand, when the feed  $CH_4/CO_2$  molar ratio was increased to 1.5,  $CH_4$  conversion was much lower, as previously observed,

but the deactivation of the catalyst, although not drastic, was more pronounced than the one of the model mixture. The excess of methane in the feed stream seems to promote methane decomposition and therefore enhance the coking of the catalyst. This resulted in the loss of 10% and 15% conversion for  $\text{CO}_2$  and  $\text{CH}_4$ , respectively.

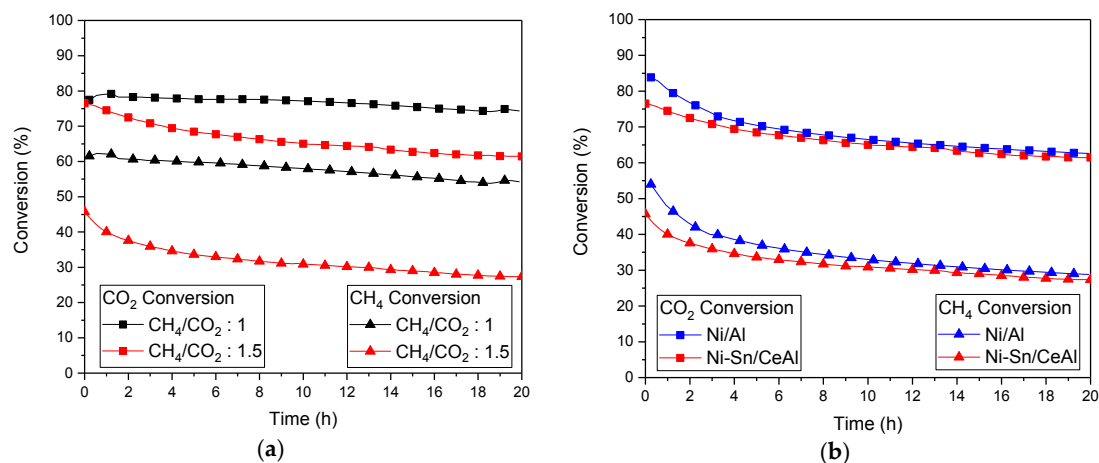


**Figure 7.** Dry reforming of methane (DRM) stability test at 650 °C on (a) Ni-Sn/CeAl at  $\text{CH}_4/\text{CO}_2$  molar ratios of 1 (model biogas) and 1.5 (sewage waste) and (b) Ni-Sn/CeAl and Ni/Al catalyst using  $\text{CH}_4/\text{CO}_2$  molar ratios of 1.5:  $\text{CO}_2$  and  $\text{CH}_4$  conversions.

The long-term test using sewage waste biogas was compared to a reference Ni/ $\text{Al}_2\text{O}_3$  catalyst on Figure 7b. The reference catalyst seems to perform slightly better than the promoted catalyst with slightly higher conversions. In fact, the introduction of Sn in the formulation of the catalyst was meant to prevent coke formation since Sn has a similar electronic configuration and was nucleating with Ni. Nevertheless, such an interaction may reduce the catalytic activity of the catalyst. Indeed, the deactivation of the reference catalysts was clearly more pronounced than that observed in the multicomponent catalyst, again highlighting the robustness of the Ni-Sn catalysts for long runs.

### 3.6. Study of Carbonaceous Deposits

Thermogravimetric analysis was conducted on the samples after reacting for 20 h to estimate the coke formation during reaction. Figure 8a shows the effect of biogas mixture on coke deposition. When subjected to the model biogas mixture, around 0.256  $\text{g}_\text{C}/\text{g}_\text{cat}$  was formed whereas for sewage derived biogas, 0.268  $\text{g}_\text{C}/\text{g}_\text{cat}$  was formed. The catalyst displayed faster deactivation under methane rich biogas, confirming that methane decomposition, as shown in Equation (3), must have been favoured, hence forming more coke on the catalyst. Figure 8b compares the carbon loading on two different catalysts after reacting with methane-rich biogas. The reference catalyst Ni/Al had similar catalytic performance to the Ni-Sn/CeAl catalyst, however, it was more prone to coking with 0.346  $\text{g}_\text{C}/\text{g}_\text{cat}$ . The multicomponent catalyst benefits from the high oxygen storage capacity of ceria that facilitates carbon oxidation [5]. In addition, Sn atoms were occupying C nucleation sites in the vicinity of Ni, preventing carbon from poisoning the active sites [16]. Moreover, the gasification of the coke present on the Ni/Al catalyst occurred at higher temperatures, suggesting the formation of more graphitic carbon as previously observed in the literature [16].

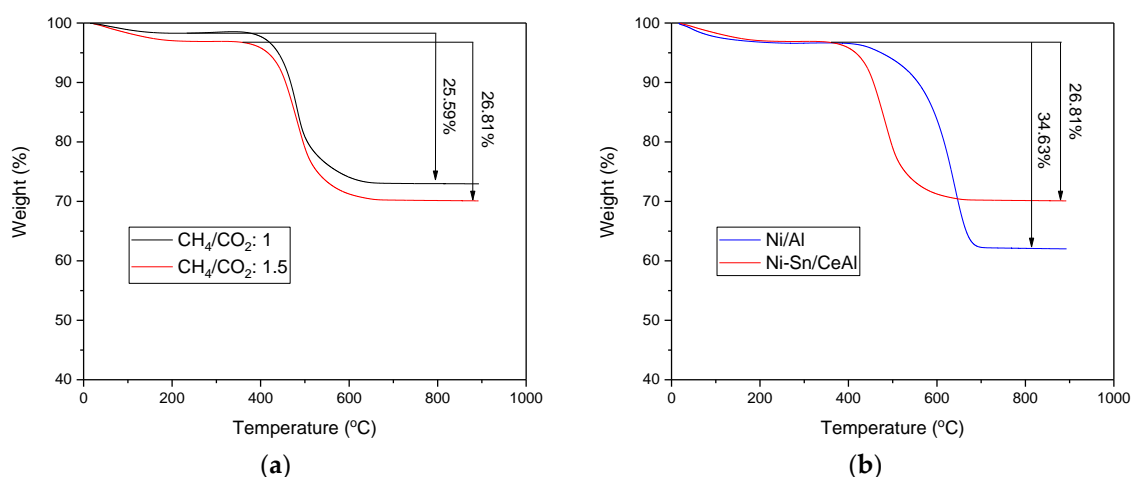


**Figure 8.** Thermogravimetric analysis for the catalysts after (a) Ni-Sn/CeAl at  $\text{CH}_4/\text{CO}_2$  molar ratios of 1 (model biogas) and 1.5 (sewage waste) and (b) Ni-Sn/CeAl and Ni/Al catalyst using  $\text{CH}_4/\text{CO}_2$  molar ratios of 1.5.

### 3.7. Post Reaction Characterisation

Figure 9 shows the XRD profiles of the Ni-Sn/CeAl catalyst after reduction, after reacting from 550 to 850 °C and after the 20 h stability run at 650 °C in a biogas ratio of  $\text{CH}_4/\text{CO}_2 = 1.5$ . The reduced sample, as described earlier, presents the characteristic peaks of  $\text{CeAlO}_3$ , Ni,  $\text{CeO}_2$  and  $\text{Al}_2\text{O}_3$ . After reacting at temperatures up to 850 °C,  $\text{CeO}_2$  seems to have completely reacted with  $\text{Al}_2\text{O}_3$  to form  $\text{CeAlO}_3$  exclusively. The high temperatures and reducing atmosphere associated with the reaction conditions favoured the phase transition. After the stability test however, the  $\text{CeO}_2$  cubic phase displayed peaks of higher intensities than those of the reduced catalyst and the post temperature screening reaction catalyst. The low temperature of the stability test, 650 °C, seems to have favoured the reverse reaction and allowed  $\text{CeAlO}_3$  to re-oxidise back to  $\text{CeO}_2$ . Indeed, the peaks associated with  $\text{CeAlO}_3$  decreased in intensity while the  $\text{CeO}_2$  diffraction peaks increased. Additionally, all post mortem samples presented a large peak at  $26^\circ$  associated to graphitic carbon. In terms of Ni crystallite size, Ni was estimated using the Scherrer equation at 17 nm, 20 nm and 11 nm in the sample reduced, after the temperature-dependant run and after the stability test, respectively. The temperature-dependant experiment was performed up to 850 °C, temperatures far above the Tammann temperature of Ni. Nickel sintering was prone to happen at such temperatures, explaining the increase in crystallite size. However, a reduction in the nickel crystallite size was observed after the 20 h stability test. First, the test took place at a much lower temperature (650 °C), which may have slowed down sintering. Second, the reaction atmosphere has an influence on the interactions amongst Ni,  $\text{CeO}_2$  and  $\text{Al}_2\text{O}_3$ . The re-oxidation of  $\text{CeAlO}_3$  to form  $\text{CeO}_2$  may have re-dispersed Ni crystallites on the catalyst surface. Zou et al. observed the same phenomenon on a Ni/  $\text{CeO}_2$ - $\text{Al}_2\text{O}_3$  catalyst reduced at 800 °C and after 105 h reaction at 350 °C. It appears Ni crystallites were re-constructed on the catalyst surface under the reaction atmosphere [27].

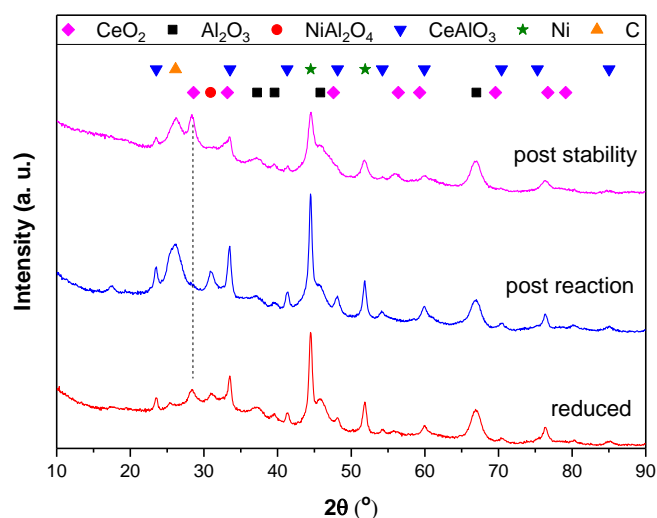


**Figure 9.** XRD characterisation spectra for Ni-Sn/CeAl reduced, post reaction and post stability at a  $\text{CH}_4/\text{CO}_2$  molar ratio of 1.5.

#### 4. Conclusions

In this work, a high performing Ni-Sn/CeO<sub>2</sub>-Al<sub>2</sub>O<sub>3</sub> catalyst was developed for the conversion of biogas to syngas via the dry reforming of methane. The synthesised material was based on the DRM catalytic standard of Ni/Al<sub>2</sub>O<sub>3</sub>, which is an inexpensive alternative to high performing noble metal-based catalysts, and upgraded using CeO<sub>2</sub> and Sn.

The performance of the multicomponent catalyst was investigated for a range of temperatures and model biogas compositions by determining the conversion of each reactant, as well as the H<sub>2</sub>/CO ratio of the syngas produced and the H<sub>2</sub> yield. Additionally, multiple characterisation techniques were carried out on fresh, reduced and spent samples of catalyst, exhibiting the crystal structure changes and the reversible reducibility for the support.

Overall, the Ni-Sn/CeAl catalyst exhibited respectable conversions of both CO<sub>2</sub> and CH<sub>4</sub> ratios for all compositions of biogas. The effect of biogas composition on the stability of the catalyst was investigated, and although no extensive signs of deactivation were detected during 20 h, the presence of excess methane accelerated the deactivation of the catalyst due to additional methane decomposition. The stability of the catalyst was also compared with the standard Ni/Al<sub>2</sub>O<sub>3</sub>. Although both catalysts displayed similar catalytic activity, the multicomponent catalyst benefited from greater coke resistance, confirming the promotion effect of both tin and ceria.

In summary, our multicomponent catalyst is a suitable material—highly active and considerably stable—to be implemented in a biogas upgrading unit to generate renewable energy (i.e., using a SOFC) or added-value products using syngas as a platform chemical.

**Author Contributions:** Conceptualization, T.R.R. & B.A.H.; methodology, L.P.-P.; formal analysis, E.I.S.; investigation, S.J. & E.I.S.; writing—original draft preparation, S.J.; writing—review and editing, E.I.S. & T.R.R.; supervision, T.R.R. & B.A.H.; funding acquisition, T.R.R.

**Funding:** This research was funded by the Department of Chemical and Process Engineering at the University of Surrey and by the EPSRC, grant EP/R512904/1 as well as the Royal Society, Research Grant RSGR1180353. LPP acknowledge Comunitat Valenciana for her APOSTD2017 fellowship. This work was also partially sponsored by the CO<sub>2</sub>Chem through the EPSRC grant EP/P026435/1.

**Acknowledgments:** The authors acknowledge Sasol for supplying the alumina support.

**Conflicts of Interest:** The authors declare no conflict of interest. The funders had no role in the design of the study; in the collection, analyses, or interpretation of data; in the writing of the manuscript, or in the decision to publish the results.

## References

1. International Energy Agency. *CO<sub>2</sub> Emissions from Fuel Combustion—Highlights*; International Energy Agency: Paris, France, 2018.
2. Boucher, O.; Friedlingstein, P.; Collins, B.; Shine, K.P. The indirect global warming potential and global temperature change potential due to methane oxidation. *Environ. Res. Lett.* **2009**, *4*, 044007. [[CrossRef](#)]
3. Ahmed, S.; Lee, S.H.D.; Ferrandon, M.S. Catalytic steam reforming of biogas—effects of feed composition and operating conditions. *Int. J. Hydrogen Energy* **2015**, *40*, 1005–1015. [[CrossRef](#)]
4. Mota, N.; Alvarez-Galvan, C.; Navarro, R.; Fierro, J. Biogas as a source of renewable syngas production: Advances and challenges. *Biofuels* **2011**, *2*, 325–343. [[CrossRef](#)]
5. Le Saché, E.; Santos, J.L.; Smith, T.J.; Centeno, M.A.; Arellano-Garcia, H.; Odriozola, J.A.; Reina, T.R. Multicomponent Ni-CeO<sub>2</sub> nanocatalysts for syngas production from CO<sub>2</sub>/CH<sub>4</sub> mixtures. *J. CO<sub>2</sub> Util.* **2018**, *25*, 68–78. [[CrossRef](#)]
6. Charisiou, N.D.; Baklavaridis, A.; Papadakis, V.G.; Goula, M.A. Synthesis gas production via the biogas reforming reaction over Ni/MgO–Al<sub>2</sub>O<sub>3</sub> and Ni/CaO–Al<sub>2</sub>O<sub>3</sub> catalysts. *Waste Biomass Valoriz.* **2016**, *7*, 725–736. [[CrossRef](#)]
7. Bonura, G.; Cannilla, C.; Frusteri, F. Ceria–gadolinia supported nickel catalyst: A suitable system for dry reforming of biogas to feed a solid oxide fuel cell (SOFC). *Appl. Catal. B* **2012**, *121–122*, 135–147. [[CrossRef](#)]
8. Lanzini, A.; Leone, P. Experimental investigation of direct internal reforming of biogas in solid oxide fuel cells. *Int. J. Hydrogen Energy* **2010**, *35*, 2463–2476. [[CrossRef](#)]
9. Shiratori, Y.; Ijichi, T.; Oshima, T.; Sasaki, K. Internal reforming of biogas on SOFC. *Int. J. Hydrogen Energy* **2010**, *35*, 7905–7912. [[CrossRef](#)]
10. Fuerte, A.; Valenzuela, R.X.; Escudero, M.J.; Daza, L. Study of a SOFC with a bimetallic Cu–Co–CeO<sub>2</sub> anode directly fuelled with simulated biogas mixtures. *Int. J. Hydrogen Energy* **2014**, *39*, 4060–4066. [[CrossRef](#)]
11. Le Saché, E.; Pastor-Pérez, L.; Watson, D.; Sepúlveda-Escribano, A.; Reina, T.R. Ni stabilised on inorganic complex structures: Superior catalysts for chemical CO<sub>2</sub> recycling via dry reforming of methane. *Appl. Catal. B* **2018**, *236*, 458–465. [[CrossRef](#)]
12. Pakhare, D.; Spivey, J. A review of dry (CO<sub>2</sub>) reforming of methane over noble metal catalysts. *Chem. Soc. Rev.* **2014**, *43*, 7813–7837. [[CrossRef](#)]
13. Shah, Y.T.; Gardner, T.H. Dry reforming of hydrocarbon feedstocks. *Catal. Rev. Sci. Eng.* **2014**, *56*, 476–536. [[CrossRef](#)]
14. Charisiou, N.D.; Siakavelas, G.; Papageridis, K.N.; Baklavaridis, A.; Tzounis, L.; Avraam, D.G.; Goula, M.A. Syngas production via the biogas dry reforming reaction over nickel supported on modified with CeO<sub>2</sub> and/or La<sub>2</sub>O<sub>3</sub> alumina catalysts. *J. Nat. Gas Sci. Eng.* **2016**, *31*, 164–183. [[CrossRef](#)]
15. Wang, S.; Lu, G.Q. Role of CeO<sub>2</sub> in Ni/CeO<sub>2</sub>–Al<sub>2</sub>O<sub>3</sub> catalysts for carbon dioxide reforming of methane. *Appl. Catal. B* **1998**, *19*, 267–277. [[CrossRef](#)]
16. Stroud, T.; Smith, T.J.; Le Saché, E.; Santos, J.L.; Centeno, M.A.; Arellano-Garcia, H.; Odriozola, J.A.; Reina, T.R. Chemical CO<sub>2</sub> recycling via dry and bi reforming of methane using Ni–Sn/Al<sub>2</sub>O<sub>3</sub> and Ni–Sn/CeO<sub>2</sub>–Al<sub>2</sub>O<sub>3</sub> catalysts. *Appl. Catal. B* **2018**, *224*, 125–135. [[CrossRef](#)]
17. San-José-Alonso, D.; Juan-Juan, J.; Illán-Gómez, M.J.; Román-Martínez, M.C. Ni, CO and bimetallic Ni–CO catalysts for the dry reforming of methane. *Appl. Catal. A* **2009**, *371*, 54–59. [[CrossRef](#)]
18. Zhang, J.; Wang, H.; Dalai, A.K. Development of stable bimetallic catalysts for carbon dioxide reforming of methane. *J. Catal.* **2007**, *249*, 300–310. [[CrossRef](#)]
19. Crisafulli, C.; Scire, S.; Minicò, S.; Solarino, L. Ni–Ru bimetallic catalysts for the CO<sub>2</sub> reforming of methane. *Appl. Catal. A* **2002**, *225*, 1–9. [[CrossRef](#)]
20. Crisafulli, C.; Scire, S.; Maggiore, R.; Minicò, S.; Galvagno, S. CO<sub>2</sub> reforming of methane over Ni–Ru and Ni–Pd bimetallic catalysts. *Catal. Lett.* **1999**, *59*, 21–26. [[CrossRef](#)]
21. Boldrin, P.; Ruiz-Trejo, E.; Mermelstein, J.; Bermúdez Menéndez, J.M.; Ramírez Reina, T.; Brandon, N.P. Strategies for carbon and sulfur tolerant solid oxide fuel cell materials, incorporating lessons from heterogeneous catalysis. *Chem. Rev.* **2016**, *116*, 13633–13684. [[CrossRef](#)]
22. Guharoy, U.; Le Saché, E.; Cai, Q.; Reina, T.R.; Gu, S. Understanding the role of Ni–Sn interaction to design highly effective CO<sub>2</sub> conversion catalysts for dry reforming of methane. *J. CO<sub>2</sub> Util.* **2018**, *27*, 1–10. [[CrossRef](#)]

23. Lau, C.S.; Tsolakis, A.; Wyszynski, M.L. Biogas upgrade to syn-gas ( $H_2$ -CO) via dry and oxidative reforming. *Int. J. Hydrogen Energy* **2011**, *36*, 397–404. [[CrossRef](#)]
24. Tao, K.; Shi, L.; Ma, Q.; Wang, D.; Zeng, C.; Kong, C.; Wu, M.; Chen, L.; Zhou, S.; Hu, Y.; et al. Methane reforming with carbon dioxide over mesoporous nickel–alumina composite catalyst. *Chem. Eng. J.* **2013**, *221*, 25–31. [[CrossRef](#)]
25. Yang, L.; Pastor-Pérez, L.; Gu, S.; Sepúlveda-Escribano, A.; Reina, T.R. Highly efficient Ni/CeO<sub>2</sub>-Al<sub>2</sub>O<sub>3</sub> catalysts for CO<sub>2</sub> upgrading via reverse water-gas shift: Effect of selected transition metal promoters. *Appl. Catal. B* **2018**, *232*, 464–471. [[CrossRef](#)]
26. Li, P.-P.; Lang, W.-Z.; Xia, K.; Yan, X.; Guo, Y.-J. The promotion effects of Ni on the properties of Cr/Al catalysts for propane dehydrogenation reaction. *Appl. Catal. A* **2016**, *522*, 172–179. [[CrossRef](#)]
27. Zou, X.; Wang, X.; Li, L.; Shen, K.; Lu, X.; Ding, W. Development of highly effective supported nickel catalysts for pre-reforming of liquefied petroleum gas under low steam to carbon molar ratios. *Int. J. Hydrogen Energy* **2010**, *35*, 12191–12200. [[CrossRef](#)]
28. Luisetto, I.; Tuti, S.; Battocchio, C.; Lo Mastro, S.; Sodo, A. Ni/CeO<sub>2</sub>-Al<sub>2</sub>O<sub>3</sub> catalysts for the dry reforming of methane: The effect of CeAlO<sub>3</sub> content and nickel crystallite size on catalytic activity and coke resistance. *Appl. Catal. A* **2015**, *500*, 12–22. [[CrossRef](#)]
29. Penkova, A.; Bobadilla, L.; Ivanova, S.; Domínguez, M.I.; Romero-Sarria, F.; Roger, A.C.; Centeno, M.A.; Odriozola, J.A. Hydrogen production by methanol steam reforming on NiSn/MgO-Al<sub>2</sub>O<sub>3</sub> catalysts: The role of mgo addition. *Appl. Catal. A* **2011**, *392*, 184–191. [[CrossRef](#)]
30. Izquierdo, U.; Barrio, V.L.; Requies, J.; Cambra, J.F.; Guemez, M.B.; Arias, P.L. Tri-reforming: A new biogas process for synthesis gas and hydrogen production. *Int. J. Hydrogen Energy* **2013**, *38*, 7623–7631. [[CrossRef](#)]
31. Chattanathan, S.A.; Adhikari, S.; McVey, M.; Fasina, O. Hydrogen production from biogas reforming and the effect of H<sub>2</sub>S on CH<sub>4</sub> conversion. *Int. J. Hydrogen Energy* **2014**, *39*, 19905–19911. [[CrossRef](#)]



© 2019 by the authors. Licensee MDPI, Basel, Switzerland. This article is an open access article distributed under the terms and conditions of the Creative Commons Attribution (CC BY) license (<http://creativecommons.org/licenses/by/4.0/>).